Optical Three-axis Tactile Sensor for Robotic Fingers

Masahiro Ohka[1], Jumpei Takata[2], Hiroaki Kobayashi[3], Hirofumi Suzuki[4],
Nobuyuki Morisawa[1] and Hanafiah Bin Yussof[1,5]

[1]*Nagoya University,*
[2]*Olympus, Co.,*
[3]*Toyota Industry, Co.,*
[4]*Honda, Co.,*
[5]*Universiti Tehnologi MARA*
[1,2,3,4]*Japan*
[5]*Malaysia*

1. Introduction

Tactile sensors capable of sensing normal and shearing force produced on a robotic finger and an object are useful for fitting a dextrose hand that can be applied to tasks that require human-like handling. Examples include such manufacturing tasks as assembly, disassembly, inspection, and materials handing. Especially in the case of humanoid robots, grasping slippery or flexible objects is required in living environments for human beings in contrast to industrial robots that handle standardized objects in controlled environments. Since the three-axis tactile sensor is effective in such cases, its importance will increase with improvements in humanoid robots.

A hemispherical tactile sensor is developed for general-purpose use with our three-axis tactile sensor that is mounted on the fingertips of a multi-fingered hand. The present three-axis tactile sensor is comprised of an acrylic dome, a light source, an optical fiber scope, and a CCD camera. The light emitted from the light source is directed onto the edge of the hemispherical acrylic dome through optical fibers. The sensing elements are concentrically arranged on the acrylic dome.

In the following sections, after conventional tactile sensors are summarized to compare the present tactile sensor's merits and demerits with conventional tactile sensors,' the principle of the three-axis tactile sensor is described. Then the basic sensing characteristics are examined for evaluating the present tactile sensor. Not only normal and shearing force sensing but also repeatability is examined in a series of experiments. Finally, surface scanning and object manipulation with one finger are shown to verify the applicability of the present tactile sensor to multi-fingered hands.

2. Short survey of tactile sensors

The importance of tactile sensors was first emphasized in 1982 by Harmon (Harmon, 1982). In this paper, human hand-like properties were desired in addition to functions of

distributed logic array. Based on questionnaires of robot engineers, he summarized such specifications of tactile sensors as a 10 x 10 array size, 1 – 10 ms response time, a wide dynamic range of 1:1000, linearity, and a skin-like surface.

So far, various tactile sensors have been developed on the basis of several physical phenomena, such as the piezoresistance effect (Ohka, M. et al., 1994; Takeuchi et al., 1994), the capacitance variation (Novak, J. L., 1989), the piezoelectric effect (Dario et al., 1984; Bicchi et al., 1989; Howe & Cutkosky, 1993; Yamada & Cutkosky, 1994), the resistance variation of conductive rubber (Raibert & Tanner, 1982; Shimojo & Ishikawa, 1990), magnetic variation (Hackwood et al., 1983), and the optical effect(Mott et al., 1984; Tanie et al., 1986; Nicholls, 1990; Maekawa, 1992; Borovac et al., 1996). However, even today, multirole tactile sensors have not been developed since every tactile sensor has both merits and demerits. For example, although semiconductor type tactile sensors utilizing the piezoresistance effect possess good linearity and can internally incorporate data processing functions with IC technology, they are fragile. Such fragility is fatal since tactile sensing intrinsically requires contact between the finger surface and an object. While conductive rubber-type tactile sensors possess such excellent characteristics as large detective area and skin-like soft surface, they emit spontaneous noise generated by the chattering of carbon particles distributed in the rubber medium and also have hysteresis.

Although optical effect type tactile sensors (hereafter, optical tactile sensor) possess several defects as well, they can be easily produced using simple equipment and Charge Coupled Device (CCD) cameras and image data processing, which are mature techniques. Thus we developed an optical three-axis tactile sensor based on the principle of an optical uniaxial tactile sensor comprised of an optical waveguide plate, made of transparent acrylic and illuminated along its edge by a light source (Mott et al., 1984; Tanie et al., 1986; Nicholls, 1990; Maekawa, 1992). As shown in Fig. 1, the light directed into the plate remains within it due to the total internal reflection generated because the plate is surrounded by air, which has a lower refractive index than the plate. A rubber sheet featuring an array of conical feelers is placed on the plate to maintain array surface contact. If an object contacts the back of the rubber sheet and produces contact pressure, the feelers collapse, and at the points where these feelers collapse, light is diffusely reflected out of the reverse surface of the plate. The distribution of contact pressure is calculated from the bright areas viewed from the plate's reverse surface.
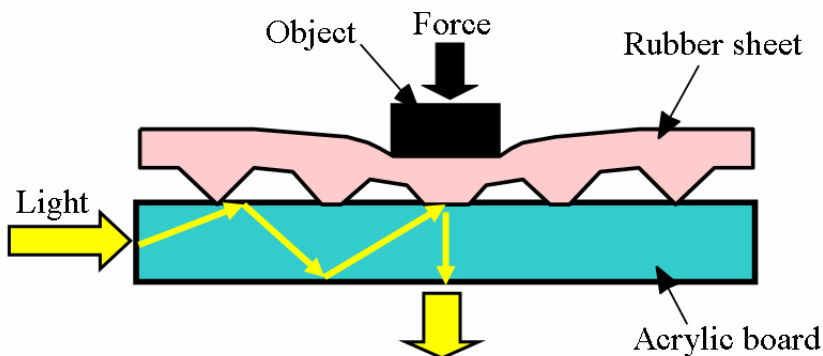

Fig. 1. Conventional optical tactile sensor

Improving the uniaxial tactile sensor to design a three-axis tactile sensor is possible. A new sensing element for it has been developed based on previous investigations (Ohka et al., 1995; Ohka et al., 2004a; Ohka et al., 2004b; Ohka et al., 2005c); it has a columnar feeler and four conical feelers that maintain contact with the acrylic surface while the tip of the columnar feeler touches an object. Normal and shearing forces applied to the columnar feeler tip are calculated from the area-sum and area-difference for the contact areas, respectively. An optical three-axis tactile sensor for micro robots was developed on the basis of simplified structure with a miniaturization advantage (Ohka et al., 2005b). Using simple rubber sheets having only a conical feeler array and an image processing technique, normal and shearing forces are calculated from the integrated grayscale value and the movement of its centroid, respectively. However, these three-axis tactile sensors can approach an object surface within limited direction due to their flat surfaces.

3. Sensing principle of optical three-axis tactile sensor

3.1 Structure of the present optical tactile sensor

The flat surface type tactile sensor described in the previous section is improved to be a hemispherical tactile sensor, which we intend to mount on the fingertips of a multi-fingered hand, as shown in Fig. 2 (Ohka et al., 2005c; Ohka et al., 2006). The multi-fingered robotic hand for general-purpose use in robotics that includes links, fingertips equipped with the three-axis tactile sensor, and microactuators (YR-KA01-A000, Yasukawa). Each microactuator consists of an AC servo motor, a harmonic drive, and an incremental encoder and is particularly developed for multi-fingered hand applications.
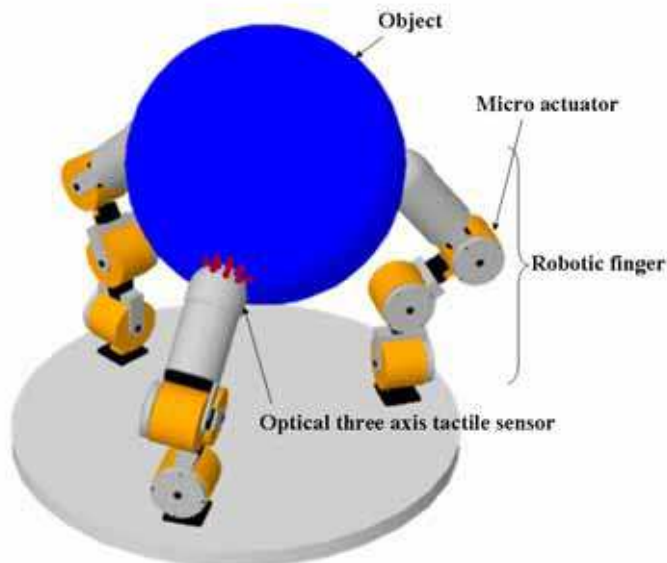

Fig. 2. Rendering of a three fingered hand equipped with optical three-axis tactile sensors

Since the tactile sensor essentially requires a lens system, it is difficult to make it be thinner, so it should be designed as an integral type of a fingertip and a hemispherical three-axis tactile sensor, as shown in Fig. 3. It is composed of a fiberscope, an acrylic dome, a fixing dome, optical fibers and 41 sensing elements. The sensing element comprised of a columnar feeler and eight conical feelers is adopted, because the element showed wide measuring range and good linearity in a previous paper (Ohka et al., 2005c). The sensing elements are made of silicone rubber (KE119, Shinetsu Co.) and are designed to maintain contact with the conical feelers and the acrylic board and to make the columnar feelers touch an object. Each columnar feeler features a flange to fit it into a counter bore portion in the fixing dome to protect the columnar feeler from horizontal displacement caused by shearing force.

Figure 4 shows a schematic view of the present tactile processing system to explain the sensing principle. The light emitted from the light source is directed into the acrylic dome through the optical fiber. Contact phenomena are observed as image data, acquired by the CCD camera through a bore scope guide and the fiberscope, and transmitted to the computer to calculate the three-axis force distribution.
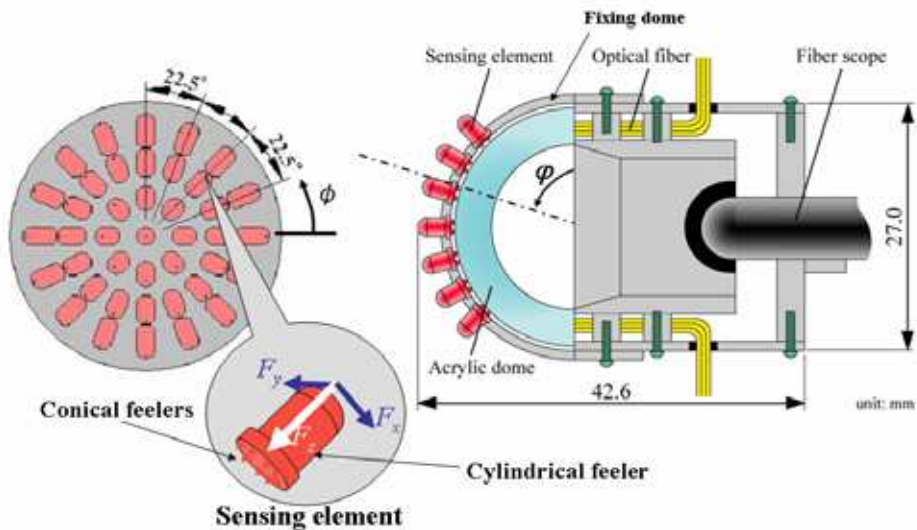

Fig. 3. Design of a fingertip including optical three-axis tactile sensor

3.2 Expressions for sensing element located on vertex

Dome brightness is inhomogeneous because the edge of the dome is illuminated and light converges on its parietal region. Since the optical axis coincides with the center line of the vertex, the apparent image of the contact area changes based on the sensing element's latitude. Although we must consider the above problems to formulate a series of equations for the three components of force, the most basic case sensing element located on the vertex will be considered first.

Coordinate O-xyz is adopted, as shown in Fig. 5. Based on previous studies (Ohka et al., 2005c), since grayscale value $g(x, y)$ obtained from the image data is proportional to pressure $p(x, y)$ caused by contact between the acrylic dome and the conical feeler, normal

force is calculated from integrated grayscale value G. Additionally, shearing force is proportional to the centroid displacement of the grayscale value. Therefore, the F_x, F_y, and F_z values are calculated using integrated grayscale value G and the horizontal displacement of the centroid of grayscale distribution $\mathbf{u} = u_x\mathbf{i} + u_y\mathbf{j}$ as follows:
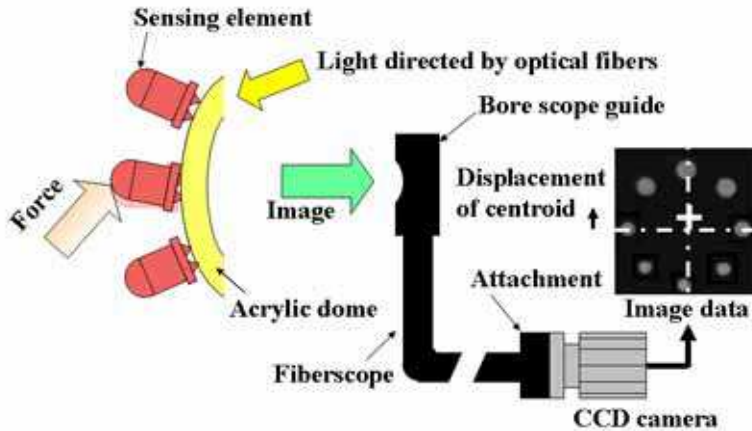

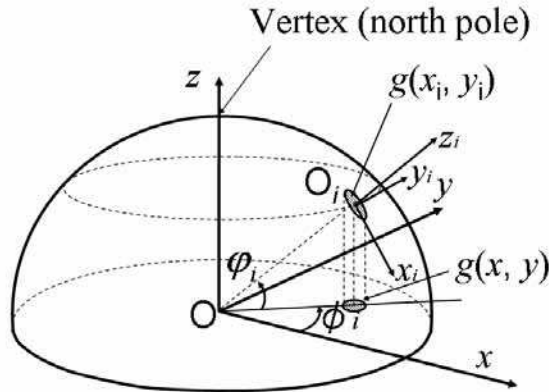Fig. 4. Principle of three-axis tactile sensor system

Fig. 5. Relationship between spherical and Cartesian coordinates

$$F_x = f_x(u_x), \tag{1}$$

$$F_y = f_y(u_y), \tag{2}$$

$$F_z = -g(G) \tag{3}$$

where $\mathbf{i}$ and $\mathbf{j}$ are the orthogonal base vectors of the x- and y-axes of a Cartesian coordinate, respectively, and $f_x(x)$, $f_y(x)$, and $g(x)$ are approximate curves estimated in calibration experiments.

3.3 Expressions for sensing elements other than those located on vertex

For sensing elements other than those located on the vertex, each local coordinate O_i-$x_iy_iz_i$ is attached to the root of the element, where suffix i denotes element number. Each z_i-axis is aligned with the center line of the element and its direction is along the normal direction of the acrylic dome. The z_i-axis in local coordinate O_i-$x_iy_iz_i$ is taken along the center line of sensing element i so that its origin is located on the crossing point of the center line and the acrylic dome's surface and its direction coincides with the normal direction of the acrylic dome. If the vertex is likened to the North Pole, the directions of the x_i- and y_i-axes are north to south and west to east, respectively. Since the optical axis direction of the CCD camera coincides with the direction of the z-axis, information of every tactile element is obtained as an image projected into the O-xy plane. The obtained image data $g(x,y)$ should be transformed into modified image $g(x_i,y_i)$, which is assumed to be taken in the negative direction of the z_i-axis attached to each sensing element. The transform expression is derived from the coordinate transformation of the spherical coordinate to the Cartesian coordinate as follows:

$$g(x_i,y_i) = g(x,y)/\sin\varphi_i . \tag{4}$$

Centroid displacements included in Eqs (1) and (2) $u_x(x,y)$ and $u_y(x,y)$ should be transformed into $u_x(x_i,y_i)$ and $u_y(x_i,y_i)$ as well. In the same way as Eq. (4), the transform expression is derived from the coordinate transformation of the spherical coordinate to the Cartesian coordinate as follows:

$$u_x(x_i,y_i) = \frac{u_x(x,y)\cos\phi_i + u_y(x,y)\sin\phi_i}{\sin\varphi_i} , \tag{5}$$

$$u_y(x_i,y_i) = u_x(x,y)\sin\phi_i + u_y(x,y)\cos\phi_i . \tag{6}$$

4. Basic sensing characteristics

4.1 Experimental apparatus

We developed a loading machine shown in Fig. 6 that includes an x-stage, a z-stage, rotary stages, and a force gauge (FGC-0.2B, NIDEC-SIMPO Co.) to detect the sensing characteristics of normal and shearing forces. The force gauge has a probe to measure force and can detect force ranging from 0 to 2 N with a resolution of 0.001 N. The positioning precisions of the y-, the z-, and rotary stages are 0.001 mm, 0.1 mm, and 0.1° , respectively.

Output of the present tactile sensor is processed by the data processing system shown in Fig. 6. The system is composed of an image processing board (Himawari PCI/ S, Library, Co.) and a computer. Image data acquired by the image processing board are processed by software made in-house. The image data acquired by the CCD camera are divided into 41 sub-regions, as shown in Fig. 7. The dividing procedure, digital filtering, integrated grayscale value and centroid displacement are processed on the image processing board. Since the image warps due to projection from a hemispherical surface, as shown in Fig. 7, software installed on the computer modifies the obtained data. The motorized stage and the force gauge are controlled by the software.
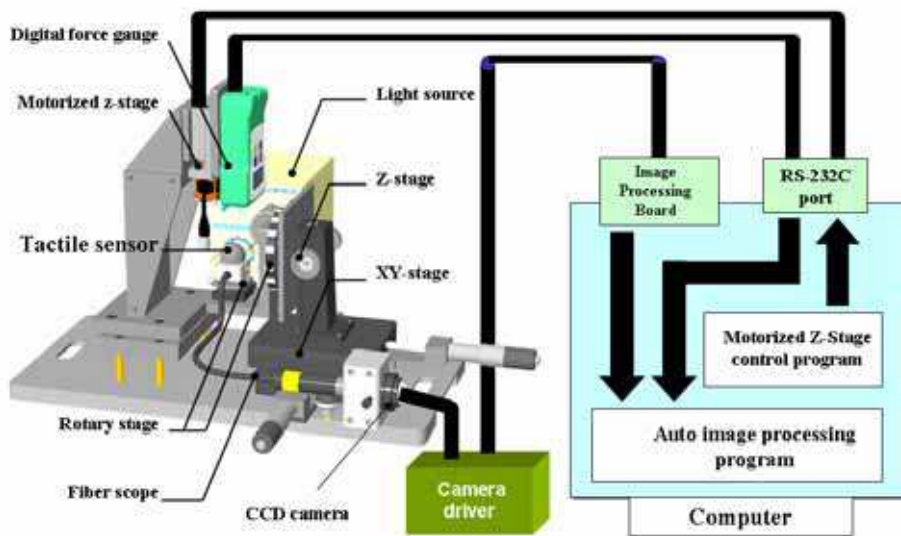
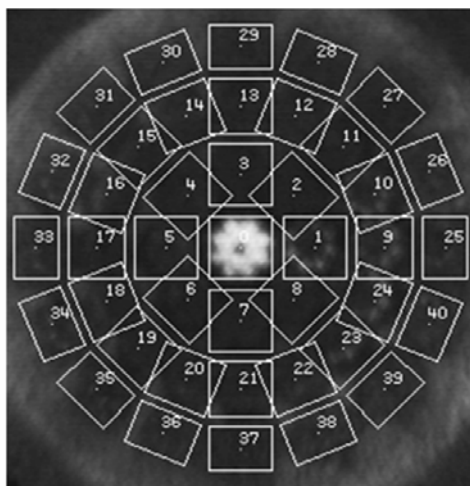Fig. 6. Loading machine and tactile data processing system

Fig. 7. Address of sensing elements

4.2 Sensing normal force

Because the present tactile sensor can detect not only normal force but also shearing force, we must confirm the sensing capability of both forces. In normal-force testing, by applying a normal force to the tip of a sensing element using the z-stage after rotating the attitude of the tactile sensor, it is easy to test the specified sensing element using the rotary stage. Since the rotary stage's center of rotation coincides with the center of the present tactile sensor's hemispherical dome, testing any sensing element aligned along the hemisphere's meridian is easy.

To evaluate the sensing characteristics of sensing elements distributed on the hemispherical dome, we need to measure the variation within the integrated grayscale values generated by the sensor elements. Figure 8 shows examples of variation in the integrated grayscale value caused by increases in the normal force for sensing element No. 0, 1, 5, 9, 17, 25, and 33. In these experiments, normal force is applied to a tip of each tactile element. As the figure indicates, the gradient of the relationship between the integrated grayscale value and applied force increases with an increase in φ; that is, sensitivity depends upon the latitude on the hemisphere. Dome brightness is inhomogeneous because the edge of the dome is illuminated and light converges on its parietal region. Brightness is represented as a function of latitude φ, and since sensitivity is uniquely determined by latitude, it is easy to modify the sensitivity according to φ.
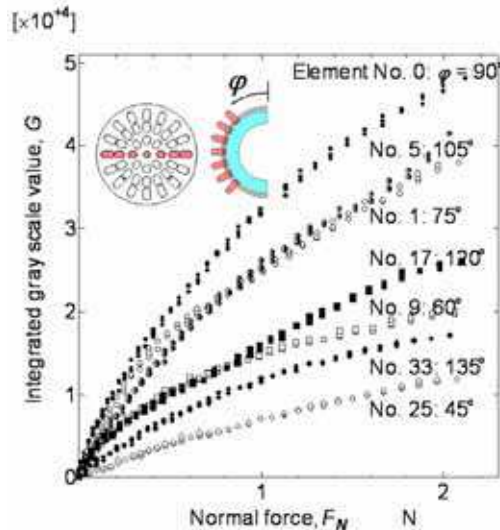

Fig. 8. Relationship between applied force and grayscale value

However, sensing elements located at the same latitude show different sensing characteristics. For example, the sensitivities of element No. 9 and 17 should coincide since they have identical latitude; however, as Fig. 8 clearly indicates, they do not. The difference reflects the inhomogeneous brightness of the acrylic dome. Therefore, we need to obtain the sensitivity of every sensing element.

When generating the shearing-force component, both the rotary and x-stages are controlled to specify the force direction and sensing element. First, the rotary stage is operated to give force direction θ. The x-stage is then adjusted to the applied tilted force at the tip of the specified sensing element. The inserted figure in Fig. 9 shows that the sensing element located on the parietal region can be assigned based on the procedure described above. After that, a force is loaded onto the tip of the sensing element using the z-stage. Regarding the manner of loading, since the force direction does not coincide with the axis of the sensing element, slippage between the probe and the tip of the sensing element occurs. To eliminate this problem, a spherical concave portion is formed on the probe surface to mate the concave portion with the hemispherical tip of the tactile element. Normal force F_N and

shearing force F_S applied to the sensing elements are calculated using the following formulas, when force F is applied to the tip of the tactile element:
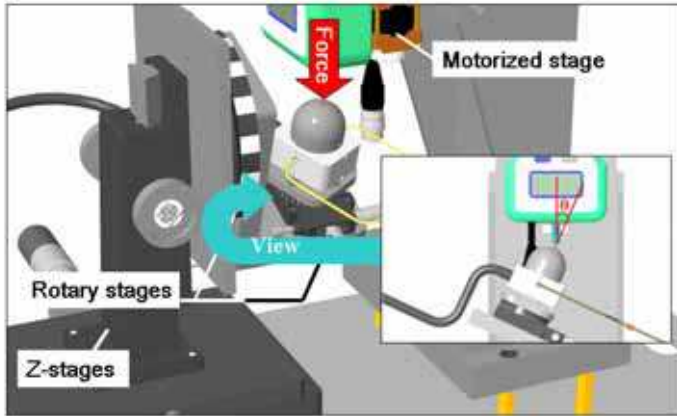

Fig. 9. Generation of shearing force component

$$F_N = F\cos\theta , \tag{7}$$

$$F_S = F\sin\theta . \tag{8}$$

To show that under combined loading condition normal force component was independently obtained with Eq. (3), we applied inclined force to the tip of the tactile element to examine the relationship between the normal component of applied force obtained by Eq. (7) and integrated grayscale value. Figure 10 displays the relationship for
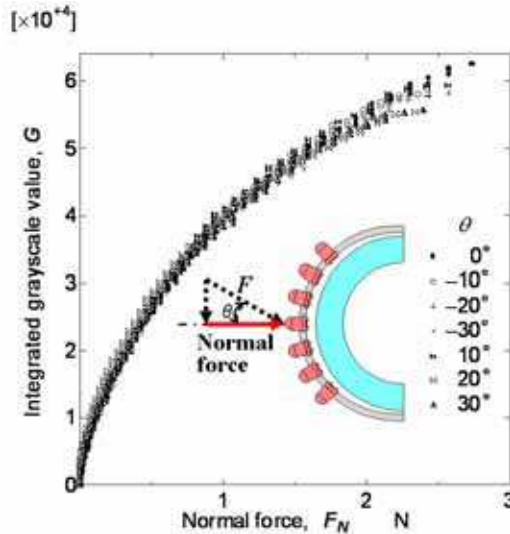

Fig. 10. Relationship between integrated grayscale value and applied normal force at several inclinations

No. 0. Even if the inclination is varied from -30 to 30°, the relationship coincides within a deviation of 3.7%. Therefore the relationship between the normal component of applied force and the integrated grayscale value is independent of inclination θ.
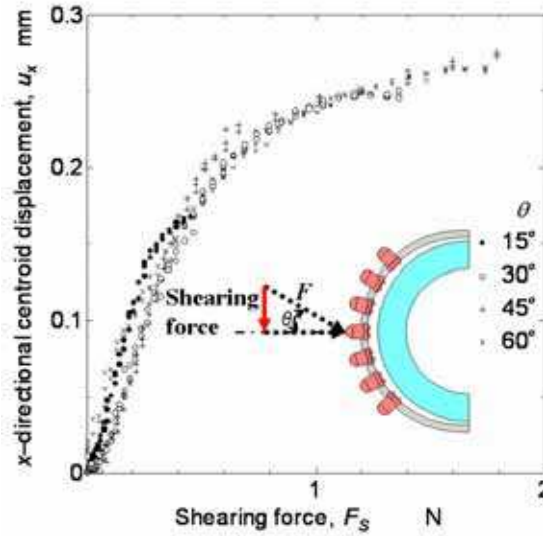

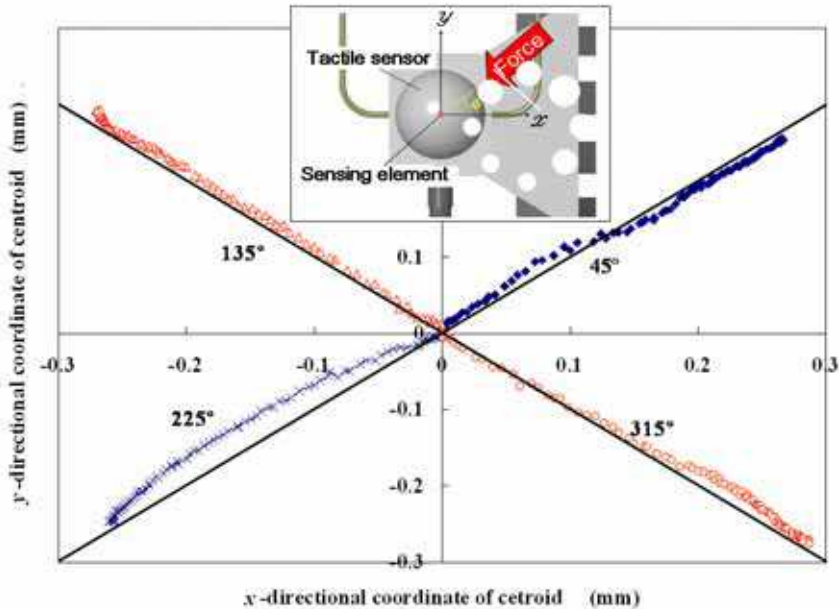Fig. 11. Relationship between centroid displacement and applied shearing force

Fig. 12. Precision of two-dimensional shearing force detection

4.2 Sensing shearing force

When force is applied to the tip of the sensing element located in the parietal region under several θ s, the relationships between the displacement of the centroid and the shearing-force component calculated by Eq. (8) are obtained, as shown in Fig. 11. Although the inclination of the applied force is varied in a range from 15 to 60°, the curves converge into a single one. Therefore, the applied shearing force is obtained independently from centroid displacement.

When the tactile element accepts directional forces of 45, 135, 225, and 315°, centroid trajectories are shown in Fig. 12 to examine shearing force detection under various directions except for the x- and y-directions. If the desired trajectories shown in Fig. 12 are compared to the experimental results, they almost trace identical desired trajectories. The present tactile sensor can detect various detections of applied force.

4.3 Repeatability

Figure 13 shows repeatability of relationship between centroid displacement and applied shearing force. The relationship between the integrated grayscale value and applied force has high repeatability. Experimental results from 1,000 repetitions on No. 8 are superimposed in Fig. 13 and show that all the curves coincide. The deviation among them is within 2%.
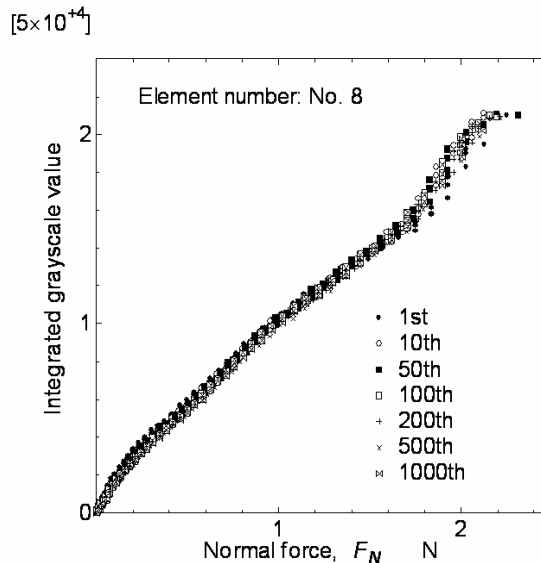

Fig. 13. Repeatability of relationship between integrated grayscale value and applied force

Contrary to normal force detection, deviation extension for shearing force is higher than for normal force, as shown in Fig. 14. The relationship between centroid movement and shearing force depends on the number of times applied force is repeated. However, if we compare the 1st to the 100th cycles, the 200th to the 500th cycles, and the 750th to the 1,000th cycles, the difference between cycles decreases with an increase of repetitions. It appears that centroid displacement is more easily disturbed and displaced by a slight change in

loading direction than the integrated grayscale value, even if the probe tip has a concave portion mated with the tip of the sensing element. Increasing the number of repetitions reduces the disturbance and stabilizes the state.
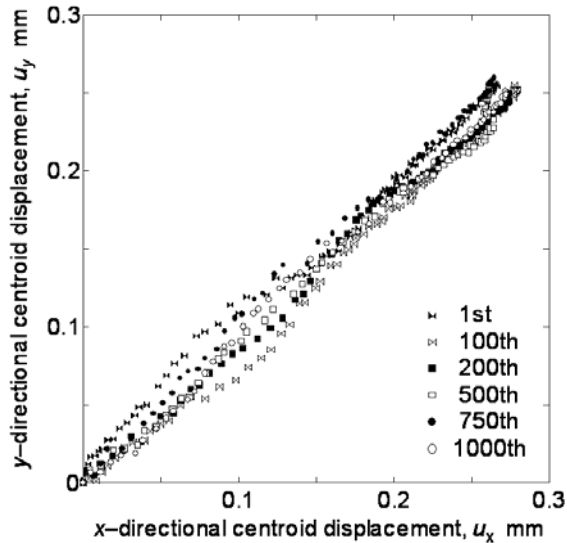

Fig. 14. Repeatability of shearing force detection

5. Robotic finger equipped with the three-axis tactile sensor

5.1 Robotic finger driven by dual computer system

A robotic finger equipped with the three-axis tactile sensor is developed to verify the present tactile sensor as shown in Fig. 15. Experiments using the finger are performed also as the first step of a series of studies on a dexterous multi-fingered hand. Since the present tactile sensor is based on image processing required heavy calculation time, a computer is used to only process image data acquired by the CCD camera. Toward a dexterous robotic hand equipped with the present tactile sensors, we develop tentatively a system of a robotic finger shown in Fig. 15, which possesses two computers; one is for tactile information processing; the other is for controlling the robotic finger; these computers are connected with a local area network.

After tactile data are obtained by the aforementioned process, they are sent to the computer for robotic finger control through the local area network. In the computer, signals applied to joint motors of the robotic finger are calculated to make the fingertip follow a trajectory according to an algorithm of Resolved Motion Rate Control (Whitney, 1969; Muir & Neuman, 1990). The signals are sent to the motor driver through the digital I/O board to drive the micro actuators.

In order to verify the robotic hand, experiments are carried out on basic motions such as surface scanning and object manipulation, which are performed in object recognition and stable grasping. Results of scanning test and object manipulation using are described in the following section.
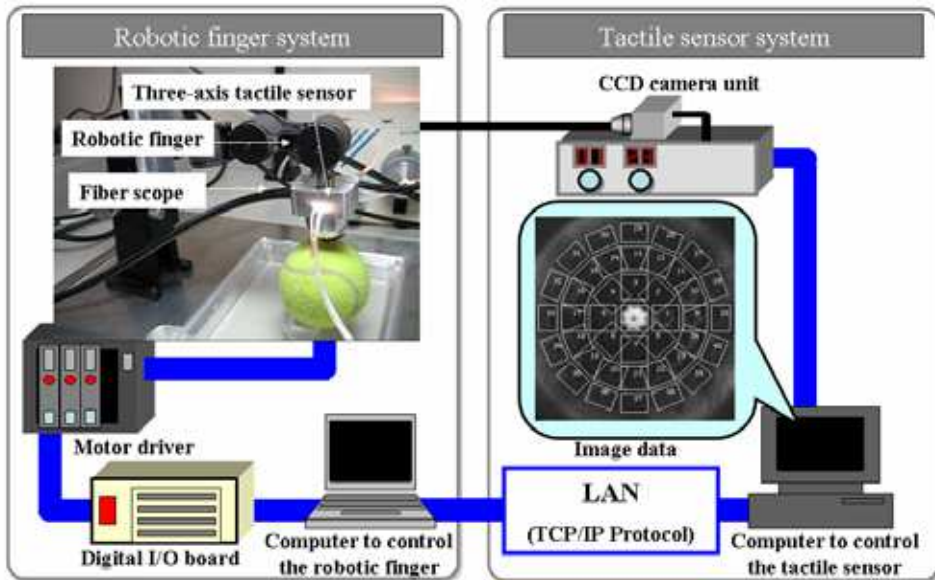
Fig. 15. Overview of the present system comprised of robotic hand and tactile data processing systems

5.2 Scanning test on flat surfaces

In scanning on a flat surface, sensing element located on the vertex of the tactile sensor is made to perpendicularly contact with a flat table by adjusting angles θ_2 and θ_3 in Fig. 16.

After that, a z-stage equipped with a robotic finger is adjusted to obtain appropriate contact force (0.1 N). Precision abrasive paper (produced by Sumitomo 3M) is mounted on the table. In this experiment, three kinds of abrasive paper, 1, 30, and 60 μ m, were adopted as specimens. To examine the dependence of friction coefficient on scanning speed, we chose three speeds: 1.4, 6.2, and 25 mm/ sec.

Variations in normal force, shearing force, and friction coefficient obtained during scanning are shown in Fig. 17 to examine the dynamic characteristics of the tactile sensor for the case of 1 μ m and 6.2 mm/ sec. Shearing force starts at zero because it is not applied at zero speed. After the start, it increases abruptly to reach a constant value. Normal force almost shows a constant value. The coefficient of friction almost shows a constant value except near the origin. The mean value of the friction coefficient is 0.39. Friction coefficients for 30 and 60 μ m abrasive paper are 0.40 and 0.53, respectively.

Next, variation in friction coefficient against variation in scanning velocity is shown in Fig. 17. In this experiment, 1 μ m abrasive paper is adopted as a specimen and eight trials are performed for each scanning speed. As shown in Fig. 18, variation in friction coefficient decreases slightly with an increase of scanning velocity. Since cutting resistance decreases with an increase of cutting speed in grinding theory, it is assumed that this cutting effect will arise in this experiment.
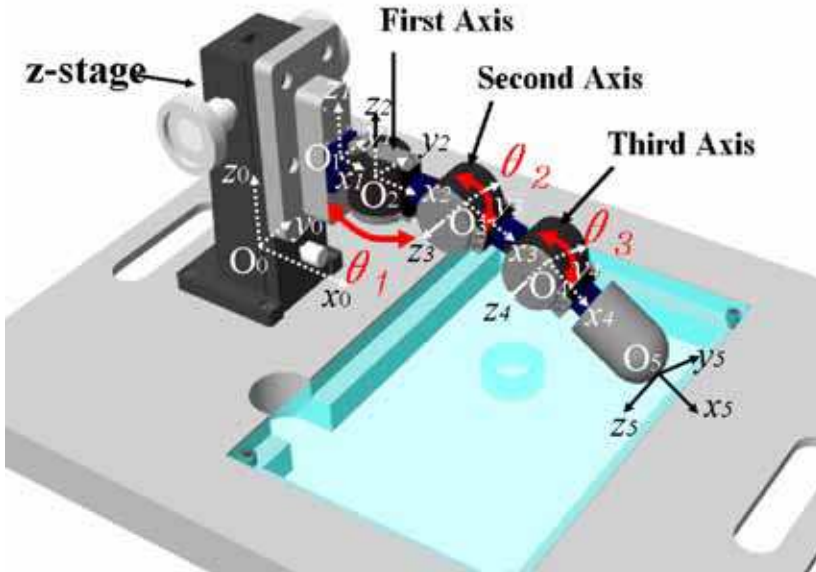
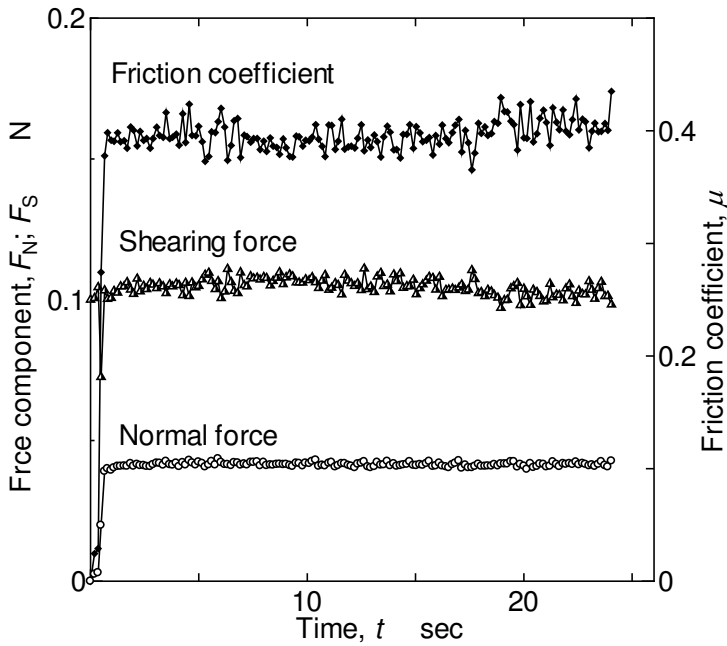Fig. 16. Robotic finger equipped with a three-axis tactile sensor

Fig. 17. Variation in force components and friction coefficient during scanning test (abrasive paper of 1 m and velocity of 6.2 mm/ sec)
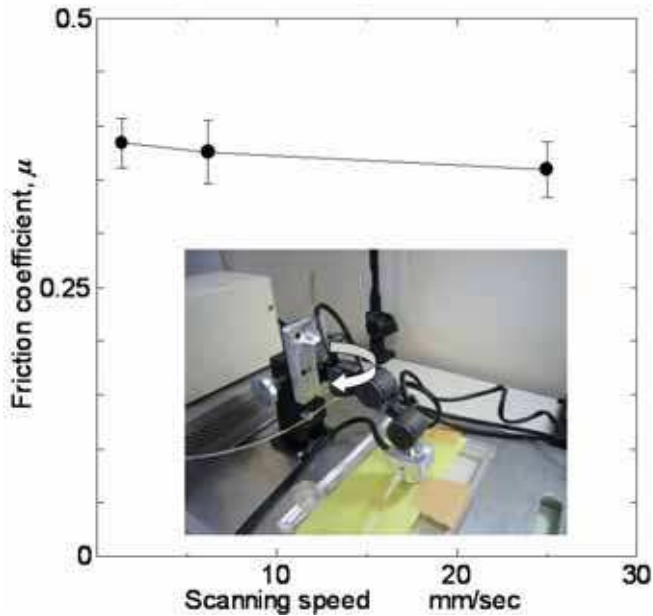
Fig. 18. Dependence of friction coefficient on scanning velocity

6.3 Object manipulation test

If slippage occurs between a finger and an object, a robotic hand cannot manipulate the object without any control based on acquired slippage information. Object manipulation tests check its capability to acquire slippage information using one-finger manipulation.

The robotic finger moves the parallelepiped object, which is put on the acrylic table (Fig. 19). Since the object is only put on the table, it is moved based on finger movement. During this manipulation, if the time derivative of the shearing force caused on the tactile sensor exceeds a specified threshold, slippage is assumed, and the finger moves slightly downward to increase compressive force. Since the sensing element is made of silicone rubber, friction between the finger and the object can be increased without considerably increasing friction between the object and the table. In this experiment, the robotic finger moves along a rectangular trajectory, and the object's movement is measured by a position sensitive detector (PSD; PS1100, Toyonaka Kenkyusyo, Co.).

Figure 20 shows the trajectory and attitude of the manipulated object. To see the attitude easier, the parallelepiped object is shown as 1/10 size in Fig. 20. As shown in Fig. 20, the object moves along the desired trajectory with considerable deviation. To analyze slippage phenomenon, variations in normal force and shearing force derivatives are shown in Fig. 21. In this experiment, since sensor elements No. 0 and 7 emit rather large signal compared to elements No. 1, 3 and 5, which touch the surface, their variations are shown in Fig. 21. Where elements such as element No. 0, 1, 3 and 5 are shown in Fig. 18. To show the relationship between the representative points of Figs. 20 and 21, corresponding points are shown in both figures as identical characters.
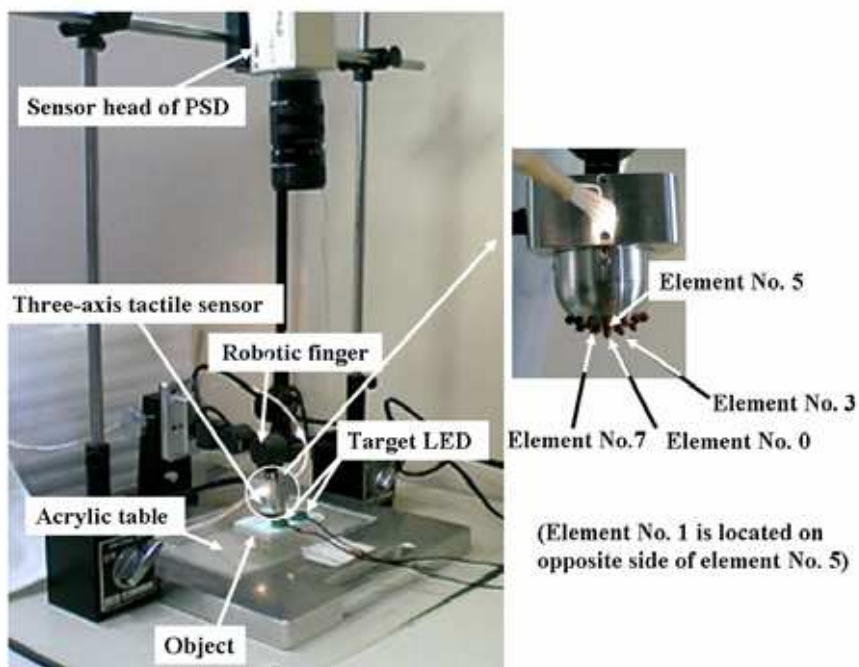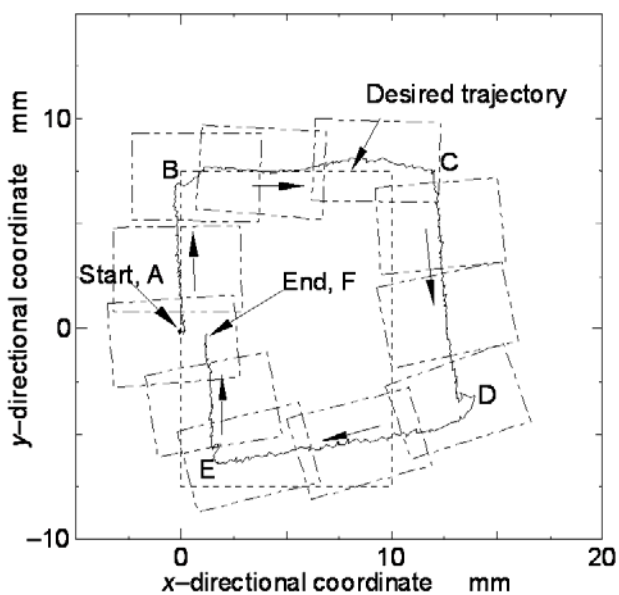
Fig. 19. Set up for object manipulations

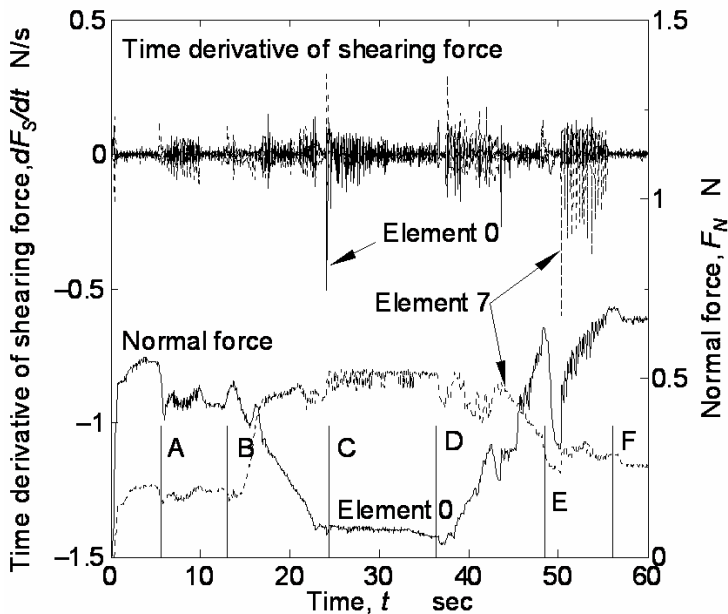Fig. 20. Manipulation of parallelepiped object

Fig. 21. Time derivative of shearing force in object manipulation

In this experiment, since finger moving starts when the compressive force exceeds 0.5 N at point A, normal force abruptly decreases just after point A in terms of the inclination of the sensing element. Since the present robotic finger only possesses three degrees of freedom and cannot control its inclination, the contact point is changed. Consequently, just after point B's normal force of element No. 0 decreases, the normal force of element No. 7 increases.

Next, we examine the time derivative of the shearing force in Fig. 21. If the derivative vibration is examined on the segments, the derivative on AB is smaller than on others. This result means that slippage on others is more considerable than on AB. Consequently, deviation after point C becomes considerable in terms of the slippage.

Through the above experimental results, the present robotic finger possesses sensing ability for acquiring the friction coefficients of the object surface and the slippage phenomenon, which are useful bits of information for a multi-fingered hand.

7. Conclusion

A new three-axis tactile sensor to be mounted on multi-fingered hands is developed based on the principle of an optical waveguide-type tactile sensor comprised of an acrylic hemispherical dome, a light source, an array of rubber sensing elements, and a CCD camera. The sensing element of the present tactile sensor includes one columnar feeler and eight conical feelers. A three-axis force applied to the tip of the sensing element is detected by the contact areas of the conical feelers, which maintain contact with the acrylic dome. Normal and shearing forces are calculated from integration and centroid displacement of the grayscale value derived from the conical feeler's contacts.

A series of experiments is conducted using a *y-z* stage, rotational stages, and a force gauge to evaluate the present tactile sensor. Although the relationship between the integrated grayscale value and normal force depended on the sensor's latitude on the hemispherical surface, it was easy to modify sensitivity based on the latitude. Sensitivity to normal and shearing forces was approximated with bi-linear curves. The results revealed that the relationship between the integrated grayscale value and normal force converges into a single curve despite the inclination of the applied force. This was also true for the relationship between centroid displacement and shearing force. Therefore, applied normal and shearing forces can be obtained independently from integrated grayscale values and centroid displacement, respectively. Also, the results for the present sensor had enough repeatability to confirm that the sensor is sufficiently sensitive to both normal and shearing forces.

Finally, the three-axis tactile sensor was mounted on a robotic finger of three degrees of freedom to evaluate the tactile sensor for dexterous hands. The robotic hand touched and scanned flat specimens to evaluate its friction coefficient. Subsequently, it manipulated a parallelepiped case put on a table by sliding it. Since the present robotic hand can perform the abovementioned tasks with appropriate precision, it is applicable to the dexterous hand in subsequent studies.

8. References

Bicchi, A.; Salisbury, J. K. & Dario, P. (1989), Augmentation of Grasp Robustness Using Intrinsic Tactile Sensing, Proc. of 1989 IEEE Int. Conf. On Robotics and Automation, 303-307.

Borovac, B.; Nagy, L. & Sabli, M. (1996), Contact Tasks Realization by sensing Contact Forces, Theory and Practice of Robots and Manipulators, Proc. of 11th CISM-IFToNN Symposium, Springer Wien New York, 381-388.

Dario, P., Rossi, D.D., Domenci, C., and Francesconi, R.(1984), Ferroelectric Polymer Tactile Sensors with Anthopomorphic Features, Proc. 1984 IEEE Int. Conf. On Robotics and Automation, pp. 332-340.

Hackwood, S.; Beni, G.; Hornak, L. A.; Wolfe, R. & Nelson, T. J(1983), Torque-Sensitive Tactile Array for Robotics, Int. J. Robotics Research, Vol. 2-2, 46-50.

Hakozaki, M. & Shinoda, H. (2002), Digital Tactile Sensing Elements Communicating Through Conductive Skin Layers, Proc. of 2002 IEEE Int. Conf. On Robotics and Automation, 3813-3817.

Harmon, L. D. (1982), Automated Tactile Sensing, The International Journal of Robotic Research, Vol. 1, No.2, 3-32.

Hosoda, K.; Tada, Y. & Asada, M. (2006), Anthropomorphic Robotic Soft Fingertip with Randomly Distributed Receptors, Robotic and Autonomous Systems, vol. 54, 104-109.

Howe, R. D. & Cutkosky, M. R. (1993), Dynamic Tactile Sensing: Perception of Fine Surface Features with Stress Rate Sensing, IEEE Trans on Robotics and Automation, Vol. 9, No. 2, 140-151.

Maekawa, H.; Tanie, K.; Komoriya, K.; Kaneko M.; Horiguchi, C. & Sugawara, T. (1992), Development of a Finger-shaped Tactile Sensor and Its Evaluation by Active Touch, in Proc. of the 1992 IEEE Int. Conf. on Robotics and Automation, 1327-1334.

Mott, H.; Lee, M. H. & Nicholls, H. R. (1984), An Experimental Very-High-Resolution Tactile Sensor Array, in Proc. 4th Int. Conf. On Robot Vision and Sensory Control, 241-250.

Muir, P. & Neuman, C. P. (1990), Resolved Motion Rate and Resolved Acceleration Servo-Control of Wheeled Mobile Robots, Proceedings of the 1990 IEEE International Conference on Robotics and Automation, Vol. 2, 1133-1140.

Nicholls, H. R. & Lee, M. H. (1989), A Survey of Robot Tactile Sensing Technology, Int. J. Robotics Res., Vol. 8-3, 3-30.

Nicholls, H. R. (1990), Tactile Sensing Using an Optical Transduction Method, Traditional and Non-traditional Robot Sensors (Edited by T. C. Henderson), Springer-Verlag, 83-99.

Novak, J. L.(1989), Initial Design and Analysis of a Capacitive Sensor for Shear and Normal Force Measurement, Proc. of 1989 IEEE Int. Conf. On Robotic and Automation, 137-145.

Ohka, M. et al. (1994), Tactile Expert System Using a Parallel-fingered Hand Fitted with Three-axis Tactile Sensors, JSME Int. J., Series C, Vol. 37, No. 1, 138-146.

Ohka, M. ,Mitsuya; Y., Takeuchi, S.; Ishihara, H. & Kamekawa, O. (1995), A Three-axis Optical Tactile Sensor (FEM Contact Analyses and Sensing Experiments Using a Large-sized Tactile Sensor), in Proc. of the 1995 IEEE Int. Conf. on Robotics and Automation, 817-824.

Ohka, M.; Mitsuya, Y.; Matsunaga, Y. & Takeuchi, S. (2004), Sensing Characteristics of an Optical Three-axis Tactile Sensor Under Combined Loading, Robotica, vol. 22, pp. 213-221.

Ohka, M.; Kawahara, T.; Kobayashi, H. & Mitsuya, Y. (2004), A Basic Study on Optical Three-axis Tactile Sensor, Eight Inter. Conf. on Manufacturing and Management, 1047-1052.

Ohka, M.; Kawamura, T.; Itahashi, T.; Miyaoka, T. & Mitsuya, Y. (2005), A Tactile Recognition System Mimicking Human Mechanism for Recognizing Surface Roughness, JSME International Journal, Series C. Vol. 48, No. 2, 278-285.

Ohka, M.; Mitsuya, Y.; Higashioka, I. & Kabeshita, H. (2005), An Experimental Optical Three-axis Tactile Sensor for Micro-robots, Robotica, vol. 23, 457-465.

Ohka, M.; Kobayashi, H. & Mitsuya, Y. (2005), Sensing Characteristics of an Optical Three-axis Tactile Sensor Mounted on a Multi-fingered Robotic Hand, IEEE/RSJ Inter. Conf. on Intelligent Robots and Systems, 1959-1964.

Ohka, M.; Kobayashi, H.; Takata, J & Mitsuya, Y. (2006), Sensing Precision of an Optical Three-axis Tactile Sensor for a Robotic Finger, Proc. of ROMAN 2006-The 15th IEEE Inter. Sympo. on Robot and Human Interactive Communication, 214-219.

Raibert, H.M. & Tanner, J.E.(1982). Design and Implementation of a VSLI Tactile Sensing Computer, Int. J Robotics Res., Vol. 1-3, 3-18.

Shimojo, M. & Ishikawa, M.; Thin and Flexible Position Sensor, J. Robotics and Mechatronics, Vol.2, No.1, pp.38-41, 1990.

Takeuchi, S.; Ohka, M. & Mitsuya, Y. (1994), Tactile Recognition Using Fuzzy Production Rules and Fuzzy Relations for Processing Image Data from Three-dimensional Tactile Sensors Mounted on a Robot Hand, Proc. of the Asian Control Conf., Vol. 3, 631-634.

Tanie, K.; Komoriya, K.; Kaneko M.; Tachi, S. & Fujiwara, A. (1986), A High-Resolution Tactile Sensor Array, Robot Sensors Vol. 2: Tactile and Non-Vision, Kempston, UK: IFS (Pubs), 189-198.

Whitney, D. E. (1969), Resolved Motion Rate Control of Manipulators and Human Prostheses, IEEE Transaction on Man-Machine Systems, Vol. 10-2, 47-53.

Yamada, Y. & Cutkosky, R. (1994), Tactile Sensor with 3-Axis Force and Vibration Sensing Function and Its Application to Detect Rotational Slip, Proc. of 1994 IEEE Int. Conf. On Robotics and Automation, 3550-3557.

Sensors: Focus on Tactile Force and Stress Sensors

Edited by Jose Gerardo Rocha and Senentxu Lanceros-Mendez

This book describes some devices that are commonly identified as tactile or force sensors. This is achieved with different degrees of detail, in a unique and actual resource, through the description of different approaches to this type of sensors. Understanding the design and the working principles of the sensors described here requires a multidisciplinary background of electrical engineering, mechanical engineering, physics, biology, etc. An attempt has been made to place side by side the most pertinent information in order to reach a more productive reading not only for professionals dedicated to the design of tactile sensors, but also for all other sensor users, as for example, in the field of robotics. The latest technologies presented in this book are more focused on information readout and processing: as new materials, micro and sub-micro sensors are available, wireless transmission and processing of the sensorial information, as well as some innovative methodologies for obtaining and interpreting tactile information are also strongly evolving.

How to reference

In order to correctly reference this scholarly work, feel free to copy and paste the following:

Masahiro Ohka, Jumpei Takata, Hiroaki Kobayashi, Hirofumi Suzuki, Nobuyuki Morisawa and Hanafiah Bin Yussof (2008). Optical Three-Axis Tactile Sensor for Robotic Fingers, Sensors: Focus on Tactile Force and Stress Sensors, Jose Gerardo Rocha and Senentxu Lanceros-Mendez (Ed.), ISBN: 978-953-7619-31-2, InTech, Available from: http://www.intechopen.com/books/sensors-focus-on-tactile-force-and-stress-sensors/optical_three-axis_tactile_sensor_for_robotic_fingers

INTECH
open science | open minds